



RESONANT FREQUENCY VARIATION OF RECTANGULAR PATCH ANTENNA DUE TO ACCUMULATION OF WATER OVER ITS SURFACE

Rajeev R. Wakodkar¹, Samik Chakraborty² and Bhaskar Gupta¹

¹Department of Electronics and Telecommunications Engineering, Jadavpur University, Kolkata, India

²Indian Maritime University, Kolkata, India

E-Mail: Rajeev_wakodkar@rediffmail.com

ABSTRACT

Microstrip or patch antennas are at the forefront of modern wireless communication revolution of the recent times. This paper investigates and proposes empirical expressions and neural network model for resonant frequency variation of rectangular patch antenna - such as one mounted flush with rooftop of a vehicle - due to accumulation of water over its surface in rainy condition. The effect is investigated for several frequency bands of interest of modern wireless communication. Empirical expressions for the change in operating frequency with respect to the accumulated water layer thickness are presented for rectangular patch antennas without radome and with radome (which is flush with patch surface) of various thicknesses. Finally, an Artificial Neural Network (ANN) is proposed as generalized model and better alternative for empirical expressions.

Keywords: rectangular patch antenna, resonant frequency, radome, vehicle rooftop mounted, water.

1. INTRODUCTION

Ubiquitous connectivity is the need of present day human society and this need is propelled by the revolutionary growth of wireless communication in recent times. Microstrip or patch antennas are at the forefront of the present day wireless communication technologies, such as mobile radio communication, Bluetooth, Wi-Fi, WiMax, Global Positioning System (GPS) etc. Microstrip (also known as patch) antennas, are one of the most widely used antenna types for modern day wireless communications, owing to the advantages they offer, such as, lightweight and small-volume, feasibilities, such as to make antenna conformal to the host surface, to manufacture using printed circuit technology for mass production at low cost and also to integrate with the circuitry where needed, etc. [1]. Rectangular microstrip antennas have the simplest geometry for analysis and design purpose and hence they are one of the commonly used types of patch antennas. Square patch antenna is a special case of rectangular patch antenna having equal width and length and useful for applications preferring dual or circular polarization, e.g. GPS.

Patch antennas can be mounted flush with rooftop of vehicles, or integrated with the roof panel at the time of manufacturing. Such patch antennas, mounted flush with rooftop of vehicle have an added advantage of aerodynamic conformability over any other antenna structure or mounting. Owing to mounting flush with rooftop, these antennas have their patch surfaces normally oriented horizontally and are exposed to outdoor environmental conditions such as snowfall in winter in some places or rain during rainy season. In rainy condition, water may be accumulated over the patch surface of these antennas due to adhesion, or if there is any small dent or depression in the rooftop at the place, where patch antenna is located. Due to adhesion, even when a patch antenna is not exactly horizontally oriented, a water

layer is formed over the patch surface or over the radome. Because water is a dielectric, its accumulation over the patch or the radome surface results in reduction of the resonant frequency [2]. A rectangular micro strip patch antenna is generally a narrowband device [1] and hence, even a small shift in its resonant frequency may lie outside the intended frequency band of use and may cause a communication failure if this fact is not taken in consideration while designing the system. In tropical regions, like India, there is a distinctly marked occurrence of rainy season. During this period, there are frequent spells of precipitations of various long and short durations. Therefore, the study of effect on resonant frequency due to accumulation of water over patch antennas, mounted flush with rooftop, assumes significance for reliable communications in today's world of 24×7, pervasive connectivity.

Water is a lossy dielectric whose relative permittivity has a complex value and it depends on the external excitation frequency, temperature and salinity [3] - [6]. There is no single model to express the permittivity of water as function of these variables and for different ranges of these variables, different models have to be used. The one suggested by Klein and Swift valid over temperature range -20 °C to 40 °C and suitable up to 10 GHz frequency is [3],

$$\varepsilon(T, S) = \varepsilon_{\infty} + \frac{\varepsilon_s(T, S)}{1 + \left(j \frac{\nu}{\nu_R(T, S)} \right)^{1-\eta}} - j \frac{\sigma(T, S)}{2\pi\varepsilon_0 \nu} \quad (1)$$

where $\varepsilon_s(T, S)$ is the static (zero frequency) dielectric constant, ε_{∞} is the dielectric constant at infinite frequency, which is constant in the Klein-Swift model, $\nu_R(T, S)$ the Debye relaxation frequency [in GHz], η the Cole-Cole



spread factor which is set to zero in the Klein-Swift model, $\sigma(T, S)$ is the conductivity of water [in $S \cdot m^{-1}$].

For rainwater, salinity S , in (1) is zero. During rainy condition in tropical countries, the ambient temperature is around 25-30°C. For a small change of say 1-2°C around temperature T , of say 25°C, relative permittivity of water found using (1) is almost constant for frequencies of interest.

Because the relative permittivity of water is frequency dependent, finding the variation in the resonant frequency of patch antenna by analytical techniques such as those described in [2], [7-16] or by simulations is quite complex and time consuming. Hence, availability of empirical relations for this purpose is quite helpful. This paper, therefore, investigates the effect on the resonant frequency due to rainwater accumulation on the patch surface by experimental methods and proposes empirical expressions for resonant frequency of rectangular patch antenna as function of water layer thickness over its patch surface for different design frequencies of antennas without radome and antennas with radome (which is flush with patch surface) of different thicknesses. ANN is better suitable for this application as it can model multivariable input-output relations using just single network, whereas empirical relations are generally suitable for single variable input-output relationship [17]. The other advantages offered by ANN are: adaptivity, fault tolerance due to parallelization, uniformity of analysis and design, neurobiological analogy, etc. [18]. Hence, this paper also presents an ANN model to find resonant frequency of a rectangular patch antenna due to accumulation of water over its radome surface having different radome thicknesses and over patch surface for antenna having no radome. The work presented here is continuation of work for a single bare patch antenna reported by the authors in [19].

The rest of the paper is organized as follows: Section 2 presents antenna design aspects of a rectangular and square patch antenna. Section 3 describes the experimental procedure to measure the resonant frequency of antenna when water layer is formed over its patch surface or the radome surface. Section 4 present results of experiments and develops empirical expressions using the experimental results for variation of resonant frequency of patch antennas for three different cases: (i) patch antennas having no radome cover (ii) patch antennas with RT duroid radome (which is flush with patch surface) and (iii) patch antenna with Teflon radome (which is flush with patch surface). Section 5 describes a comprehensive ANN model for finding the resonant frequency for all cases discussed in section 4. Finally section 6 offers concluding remarks on the work.

2. ANTENNA DESIGN ASPECTS

The patch geometries used for fabrication of antennas are rectangular and square. Five antennas, each of which has rectangular patch geometry, are fabricated by etching one of the sides of two sided copper clad 1.524 mm (60 mils) thick RT Duroid material sheet. In addition,

five more antennas with square patch shape are fabricated similarly using the same dielectric material. The dielectric constant of the RT Duroid used is 2.4 and loss tangent is 0.019. The design of microstrip patch radiator involves the computation of its patch dimensions as outlined in [1]. The resonant frequency of rectangular patch antenna for dominant TM_{10} mode is given by

$$f_r = f_{10} = \frac{c}{2L} \frac{1}{1 + \Delta} \frac{\epsilon_r}{\sqrt{\epsilon_{re}(L)\epsilon_{re}(W)}} \quad (2)$$

Where, $\epsilon_{re}(L)$ and $\epsilon_{re}(W)$ are effective dielectric constants given by

$$\epsilon_{re}(W) = \frac{\epsilon_r + 1}{2} + \frac{\epsilon_r - 1}{2} F\left(\frac{W}{h}\right) \quad (3)$$

$$\epsilon_{re}(L) = \frac{\epsilon_r + 1}{2} + \frac{\epsilon_r - 1}{2} F\left(\frac{L}{h}\right) \quad (4)$$

$$F\left(\frac{a}{h}\right) = \begin{cases} \left(1 + \frac{12h}{a}\right)^{-0.5} + 0.04\left(1 - \frac{a}{h}\right)^2 & \frac{a}{h} \leq 1 \\ \left(1 + \frac{12h}{a}\right)^{-0.5} & \frac{a}{h} \geq 1 \end{cases} \quad (5)$$

and Δ is an empirical correction factor given by

$$\Delta = \frac{h}{L} \left[0.882 + \frac{0.164(\epsilon_r - 1)}{\epsilon_r} + \frac{\epsilon_r + 1}{\pi\epsilon_r} \left\{ 0.7 + \ln\left(\frac{L}{h} + 1.88\right) \right\} \right] \quad (6)$$

Equations (2) and (6) have to be solved iteratively to find value of L and W for a given resonant frequency f_r . For square antenna, $W = L$ is taken.

The probe feed position f_p , for optimal return loss, is found by simulation using method of moments based IE3D™ software [20]. Figure-1 shows the patch dimensions and probe feed position.

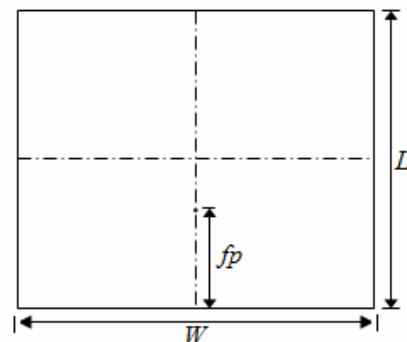


Figure-1. The dimensions (mm) of a rectangular patch area and probe feed position (mm).

Standard microwave commercial frequencies (3G and Wi-Fi) are used for design of antennas. Also some non-standard frequencies are used in order to increase the data



base required for training of ANN. The specifications of all the antennas are given in Table-1.

Table-1. Antenna specifications.

Antenna number	Resonant frequency f_{r0} (GHz)	Commercial application frequency band	W (mm) \times L (mm)	f_p (mm)
1	1.35	None	84 \times 70	23
2	1.72	3G (USA)	82 \times 55	16
3	1.93	3G (Europe)	72 \times 48	13.5
4	2.14	3G (Europe)	66 \times 44	12.5
5	2.6	3G (Europe)	54 \times 36	11
6	3.07	None	30 \times 30	10
7	3.54	Wi-Fi	26 \times 26	9
8	3.97	None	23 \times 23	8
9	4.55	None	20 \times 20	7
10	5.33	Wi-Fi (802.11a/n)	17.5 \times 17.5	5.5

For patch antenna, mounted flush with rooftop, if it is not mounted nearer to any roof edges, the large roof size will act as infinite ground plane. To simulate this infinite ground plane effect, antenna ground plane is fabricated three times the dimension of the top layer patch, or larger. Under this condition fringing effect as well as impedance and other antenna parameters dose not differ significantly from the corresponding infinite ground plane case [21].

Patch antennas, particularly when used in outdoor applications – such as those mounted flush with rooftop of vehicles – are covered by radome for protection from environmental conditions. Teflon ($\epsilon_r = 2.4$) is one of the commonly used materials for radome of antennas and RT Duroid has same electrical characteristic as Teflon ($\epsilon_r = 2.4$). Hence, these materials are used for antenna radome in this work. Thickness of Teflon sheet used is 3.05 mm and that of RT Duroid sheet is 1.524 mm.

3. EXPERIMENTAL PROCEDURE

For experimental measurements Vector Network Analyser (Agilent Technologies™, series ENA, model E5071B) is used. The network analyser is calibrated using Agilent® E-calkit 85092-60008 before measurement. The effect of rainwater accumulation over patch surface of patch antenna, which is mounted flush with rooftop of vehicle, is emulated by orienting the patch surface of antenna horizontally and pouring distilled water or stored rainwater over the horizontal microstrip patch surface to form water layer – of uniform thickness successively equal to 1, 2, 3, 4 and 5 mm – and its effect on the resonant frequency of the antenna is observed. The water is poured such that it covers the entire microstrip patch and the dielectric substrate surface as shown in Figure-2. Side enclosure walls of dielectric (a substance used for fixing glass panes to metal window frame) are formed to facilitate accumulation of water of thickness up to 5 mm.

It is observed that the dielectric walls of side enclosure have no effect on the performance of antenna as these walls are sufficiently away from the radiating edges of the patch antenna. The temperature of water is equal to room temperature (25°C) at the time of experimentation. The measurement setup is shown in the photograph of Figure-3.

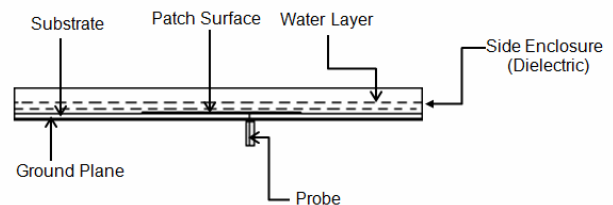


Figure-2. Side view of patch antenna covered with water layer.

Though in practical outdoor applications, patch antenna is almost always covered by radome for protection from environmental conditions, finding effects of water accumulation on resonant frequency of bare patch antennas is useful for comparison purpose and better understanding of the phenomenon of the resonant frequency variation.

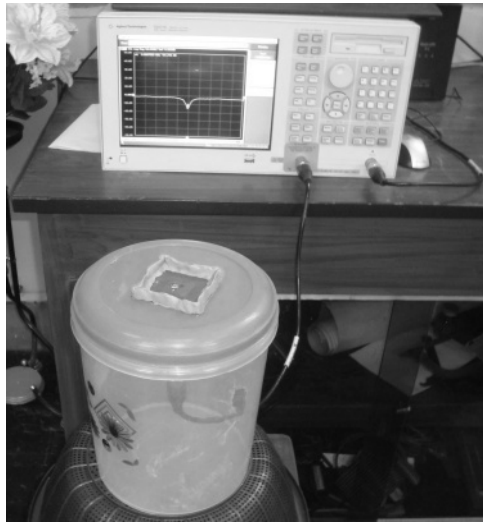


Figure-3. Photograph of experimental setup.

For finding the effect on frequency in presence of radome (which is flush with patch surface), radome sheet is placed on top of antenna and pressed against it by tight clamping to minimize the air gap between the patch surface and radome. Figure-4 shows the arrangement for this (The clamp or press mechanism is not shown in the Figure). The experiment is repeated by pouring the water over the radome surface in each case of radome as described earlier for patch antenna without radome.

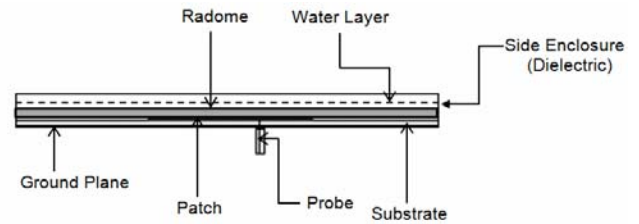


Figure-4. Side view of water layer over flush mounted radome of patch antenna.

4. OBSERVATIONS, DISCUSSIONS AND EMPIRICAL EXPRESSIONS

4.1. Observations for patch antennas (not covered with radome)

The observed values of resonant frequencies are given in Table-2. (Displayed results here are rounded to two places of digits after the decimal point). In Table-2 and the ensuing Tables, A1, A2... represents Antenna #1, Antenna # 2... etc. The corresponding observed return loss values (rounded to one place of digit after the decimal point) are as in Table-3. The graphs of resonant frequency versus water layer thickness over patch surface and corresponding fitted curves are plotted as in Figure-5.

Table-2. Observed resonant frequencies of antennas (without radome).

Water layer thickness (mm)	Resonant frequencies (GHz)									
	A1	A2	A3	A4	A5	A6	A7	A8	A9	A10
0	1.35	1.72	1.93	2.14	2.6	3.07	3.55	3.98	4.54	5.33
1	1.18	1.44	1.56	1.71	1.97	2.25	2.5	2.72	2.99	3.37
2	1.08	1.27	1.36	1.45	1.64	1.79	1.93	2.1	2.23	2.46
3	1.01	1.17	1.24	1.32	1.47	1.56	1.67	1.75	1.84	1.99
4	0.96	1.1	1.16	1.23	1.35	1.42	1.5	1.58	1.65	1.76
5	0.94	1.06	1.11	1.17	1.28	1.34	1.41	1.49	1.55	1.64

Table-3. Observed return loss at corresponding resonant frequencies in Table-2.

Water layer thickness (mm)	Return loss at corresponding resonant frequency (GHz)									
	A1	A2	A3	A4	A5	A6	A7	A8	A9	A10
0	-16.4	-17.8	-18.1	-18.2	-18.4	-19.9	-16.4	-17.2	-19.2	-16.6
1	-14	-10.7	-10.2	-11.8	-9.1	-13.5	-10.8	-10.6	-14.6	-11.2
2	-9.1	-6.1	-5.5	-7.3	-5.7	-7.2	-6.1	-4.9	-10.4	-5.1
3	-5.2	-4.4	-4.7	-4.9	-3.2	-5.1	-5.4	-4.7	-8.7	-4
4	-5	-4.2	-4	-3.5	-3.2	-4.2	-4.8	-4	-6.9	-3.7
5	-4.6	-2.9	-3.5	-2.9	-3.2	-3.8	-3.9	-3.7	-6.3	-3.1



www.arnpjournals.com

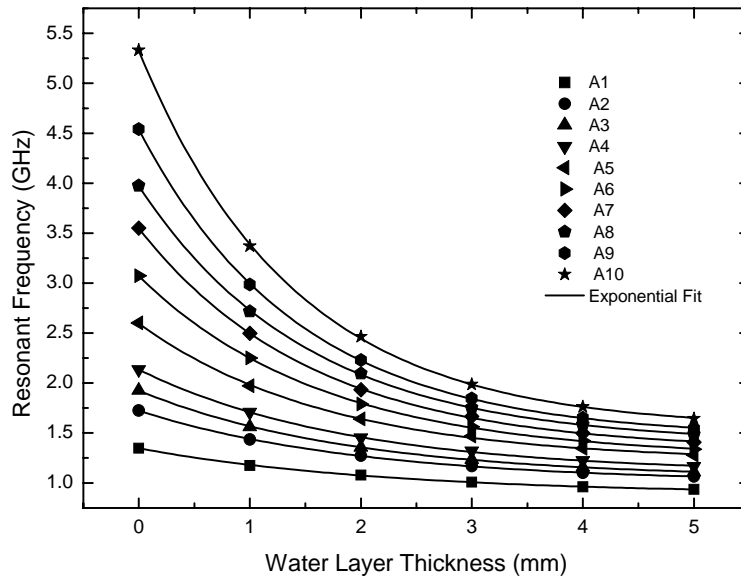


Figure-5. Resonant frequency versus water layer thickness over the patch surface

4.2. Observations for patch antennas with RT duroid radome

The observed resonant frequencies are given in Table-4 and the corresponding return loss values are given in Table-5.

Table-4. Observed resonant frequencies of antennas (with RT Duroid Radome).

Water layer thickness (mm)	Resonant frequencies (GHz)									
	A1	A2	A3	A4	A5	A6	A7	A8	A9	A10
0 ^a	1.35	1.72	1.93	2.14	2.6	3.07	3.55	3.98	4.54	5.33
0	1.32	1.7	1.9	2.11	2.57	3.04	3.51	3.95	4.53	5.31
1	1.26	1.62	1.82	2.03	2.49	2.96	3.43	3.87	4.47	5.27
2	1.23	1.58	1.78	1.99	2.44	2.91	3.38	3.83	4.44	5.25
3	1.2	1.55	1.75	1.96	2.41	2.88	3.36	3.81	4.42	5.24
4	1.19	1.53	1.73	1.94	2.39	2.86	3.34	3.79	4.41	5.24
5	1.17	1.52	1.72	1.93	2.38	2.84	3.32	3.78	4.4	5.23

^aFirst row corresponds to observations of bare patch antennas

Table-5. Observed return loss at corresponding resonant frequencies in Table-4.

Water layer thickness (mm)	Return loss at corresponding resonant frequency (GHz)									
	A1	A2	A3	A4	A5	A6	A7	A8	A9	A10
0 ^a	-16.4	-17.8	-18.1	-18.2	-18.4	-19.9	-16.4	-17.2	-19.2	-16.6
0	-14.4	-15.5	-16.5	-17.3	-14	-15.2	-14.5	-17.2	-17.6	-15.4
1	-6.3	-11.9	-13.1	-11.3	-6.1	-11	-9.8	-15.4	-14.6	-11.7
2	-3.7	-9.9	-10.2	-6.5	-5.7	-7.8	-5	-5.6	-10.4	-10.8
3	-3.7	-5.6	-7.7	-3.6	-3.2	-4.5	-3.9	-4.9	-8.7	-9.1
4	-3.7	-4.2	-3.7	-3.4	-2	-4.2	-3.2	-4.7	-6.9	-8
5	-3.3	-3.6	-3.5	-3.4	-2	-4	-2.9	-4	-6.3	-7

^aFirst row corresponds to observations of bare patch antennas



The graphs of resonant frequency versus water layer thickness over the flush mounted RT Duroid radome surface and corresponding fitted curves are plotted as in Figure-6.

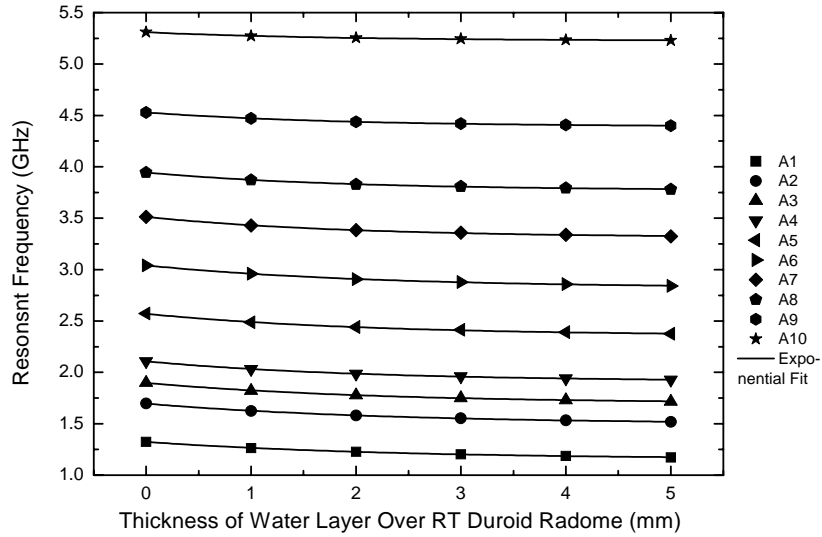


Figure-6. Resonant frequency versus thickness of water layer over the RT Duroid radome surface.

4.3. Observations for patch antennas with teflon radome

The observed resonant frequencies are given in Table-6 and the corresponding return loss values are given

in Table-7. The graphs of resonant frequency versus water layer thickness over the flush mounted Teflon radome surface and corresponding fitted curves are plotted as in Figure-7.

Table-6. Observed resonant frequencies of antennas (with Teflon Radome)

Water layer thickness (mm)	Resonant frequencies (GHz)									
	A1	A2	A3	A4	A5	A6	A7	A8	A9	A10
0 ^a	1.35	1.72	1.93	2.14	2.6	3.07	3.55	3.98	4.54	5.33
0	1.3	1.67	1.87	2.08	2.54	3.01	3.49	3.93	4.52	5.31
1	1.27	1.64	1.83	2.05	2.5	2.97	3.44	3.89	4.48	5.28
2	1.25	1.61	1.8	2.01	2.47	2.93	3.41	3.85	4.45	5.26
3	1.23	1.58	1.78	1.99	2.44	2.91	3.38	3.83	4.43	5.25
4	1.21	1.56	1.76	1.97	2.42	2.88	3.36	3.81	4.42	5.24
5	1.2	1.55	1.74	1.95	2.4	2.87	3.35	3.8	4.41	5.24

^aFirst row corresponds to observations of bare patch antennas



Table-7. Observed return loss at corresponding resonant frequencies in Table-6.

Water layer thickness (mm)	Return loss at corresponding resonant frequency (GHz)									
	A1	A2	A3	A4	A5	A6	A7	A8	A9	A10
0 ^a	-16.4	-17.8	-18.1	-18.2	-18.4	-19.9	-16.4	-17.2	-19.2	-16.6
0	-14.8	-16.1	-16.9	-17.5	-15.5	-16.7	-14.7	-15.9	-18	-15.9
1	-6.9	-12.5	-13.8	-11.7	-6.8	-11.6	10	-5.8	-15.2	-12.4
2	-4.1	-10.1	-10.3	-6.8	-5.9	-8	-5.1	-5.1	-10.7	-10.9
3	-3.9	-5.8	-7.9	-3.9	-3.3	-4.7	-4.2	-4.9	-8.8	-9.3
4	-3.7	-4.2	-4.7	-4.4	-3	-4.2	-3.2	-4.6	-7.1	-8.1
5	-3.5	-3.8	-3.6	-3.4	-2	-4.1	-3.1	-3.8	-6.4	-7.5

^aFirst row corresponds to observations of bare patch antennas

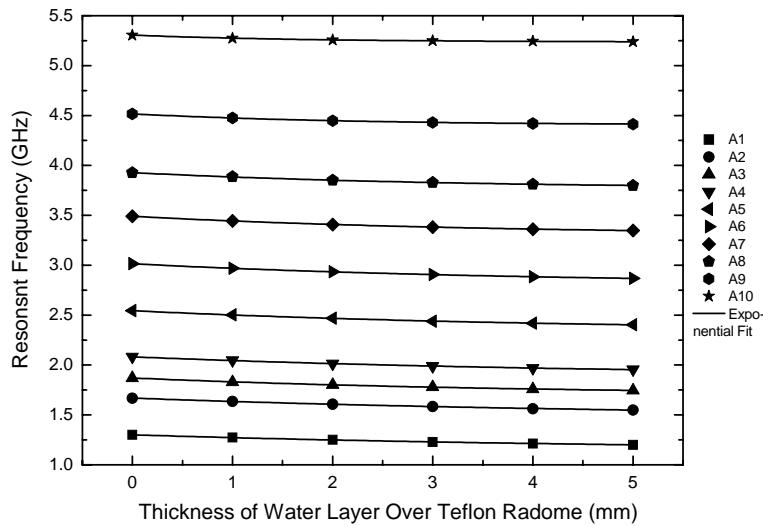


Figure-7. Resonant frequency versus thickness of water layer over the teflon radome surface.

4.4. Discussions

From the Tables-3, 5 and 7, it is observed that due to accumulation of water over the patch surface or over the radome surface, impedance match of antenna with probe worsens with increase in water layer thickness. This phenomenon is observed in case of other dielectric superstrates also [22] but in case of water, it seems to be worst because of very high dielectric constant of water. It may be improved taking the loading effect of water into account at the time of antenna design.

4.5. Empirical expressions (curve fitting)

An exponential decay model is used for curve fitting to get empirical relations between the resonant frequency and the thickness of the water layer on the rectangular microstrip patch antenna surface, for each antenna.

The general form of relation developed is

$$f_{rxh} = f_{rx\infty} + (f_{rx0} - f_{rx\infty}) * \exp\left(-\frac{h_w}{H_{wx}}\right) \quad (7)$$

Where, subscript $x = n, d$ or t , corresponds to the case of no radome, RT Duroid radome or Teflon radome, respectively.

h_w = thickness of water layer (mm)

f_{rxh} = resonant frequency (GHz) of antenna for water layer thickness of h_w for case x

f_{rx0} = resonant frequency (GHz) of antenna for water layer thickness of $h_w = 0$, i.e. no water layer for the case x

$f_{rx\infty}$ = resonant frequency (GHz) of antenna for infinitely thick water layer, i.e. saturation value of resonant frequency for the case x

H_{wx} = water layer thickness (mm) to reach saturation value of resonant frequency if the rate of change of resonant frequency due to change in water layer thickness would be constant and would be equal to initial value i.e. at $h_w = 0$ for the case x . This can be called as water layer thickness constant.



The constants f_{rx0} , $f_{rx\infty}$ and H_{wx} for the case $x = n$, d and t , for each antenna are given in Table-8. Equation (7) thus represents set of empirical expressions.

Table-8. Curve fitting parameters.

Resonant frequency (GHz)	Curve fitting parameters							
f_{rno}	$f_{r\infty}$	H_{wn}	f_{rdo}	$f_{rd\infty}$	H_{wd}	f_{rto}	$f_{rd\infty}$	H_{wt}
1.35	0.89	2.25	1.32	1.15	2.39	1.3	1.14	5.29
1.72	1.01	1.99	1.7	1.5	2.35	1.67	1.47	5.22
1.93	1.05	1.91	1.9	1.7	2.21	1.87	1.7	4.73
2.14	1.1	1.89	2.11	1.91	2.16	2.08	1.88	4.27
2.6	1.22	1.7	2.57	2.36	2.12	2.54	2.34	3.97
3.07	1.25	1.66	3.04	2.82	2.1	3.01	2.81	3.94
3.54	1.32	1.56	3.51	3.31	1.96	3.49	3.3	3.5
3.97	1.4	1.52	3.95	3.77	1.87	3.93	3.76	3.2
4.55	1.46	1.44	4.53	4.39	1.86	4.52	4.4	2.21
5.33	1.55	1.39	5.31	5.22	1.86	5.31	5.24	1.75

5. NEURAL NETWORK MODEL

Artificial Neural Network (ANN) (also known simply as Neural Networks (NN)), are the most suitable candidates for multivariable, highly nonlinear input-output data mapping, where finding some closed form of function is either too complex or does not exist and using some approximate model does not give sufficiently accurate results [17].

A neural network is a network of many simple processors comprising of units, nodes and neurons, each of which has small amount of memory. These processors are connected by unidirectional communication channels (connections) that carry numerical data. A neural network thus resembles the brain [17, 18]. Multilayer Perceptron (MLP) Architecture of ANN is by far the most popular type of ANN architecture which is capable of approximating generic classes of functions. These networks use a feed forward architecture consisting of input layer, one or more hidden layers, and an output layer, with output of each neuron in the preceding layer connected only to the input of one or more neurons in the immediately succeeding layer. These networks, trained in the supervisory error back propagation mode, have already been used in many electromagnetic engineering applications and specifically for antenna analysis and design applications [23-27]. In these networks, during training, the network adjusts its weights and biases in each iteration to minimise the error between the computed output and presented (desired) output. The network is said to be converged or trained when the error (generally Mean Square Error (MSE)) between computed and desired output is zero or less than a certain predefined value for any further successive iteration. Various algorithms exist for adapting weights and biases for faster convergence of the network. One of such back propagation algorithm, which is fast converging, is Lavenberg-Marquardt Back-

propagation (LMBP) algorithm [28]. Advantage of LMBP algorithm for function approximation problems is that, for networks that contain up to a few hundred weights, the LMBP algorithm will have the fastest convergence. This advantage is especially noticeable if very accurate training is required. In many cases, LMBP is able to obtain lower mean square errors than any of the other algorithms tested [28].

5.1. Network architecture

Proposed multilayer perceptron model of ANN is shown in Figure-8.

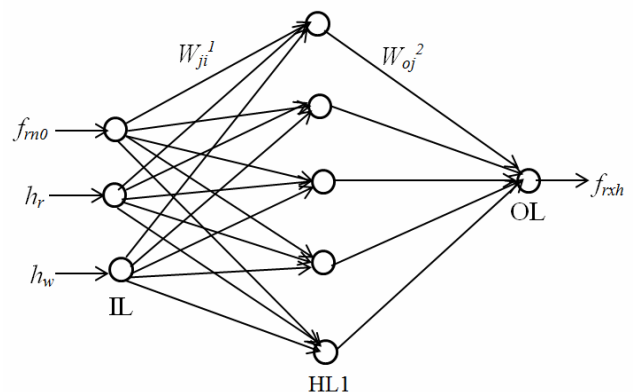


Figure-8. Proposed multilayer perceptron model of ANN.

Theoretically, MLP ANN architecture with one hidden layer and nonlinear activation function for the hidden nodes can implement any function of practical interest [17]. Hence in the proposed ANN model only one hidden layer is used. In Figure-8, IL denotes input layer. Nodes in the hidden layer and output layer perform calculations and memory function for weights and biases,



whereas, the nodes in the input layer do not perform any computation but only perform memory functions for input signal. The resonant frequency of an antenna depends upon three parameters, namely, resonant frequency of antenna, f_{rno} , (when there is no radome and no water layer over its patch surface), the radome thickness, h_r (zero in case of no radome) and water layer thickness h_w . Hence, the network has three input nodes. The desired (output) parameter is resonant frequency of the patch antenna for given combination of three input parameters, output layer OL, has one node. HL1 denotes the first (and the only one in this case) hidden layer comprising five nodes.

The rule of thumb to calculate the approximate number of hidden layer nodes is that the number of hidden layer nodes N , should satisfy the equation [17],

$$N = \frac{PT}{10(I+O)} \quad (8)$$

where PT is the number of input-output training pairs, I is the number of input layer nodes and O is the number of output layer nodes. The number of input-output pairs available from the data generated through measurement is 180. Out of which 140 randomly chosen input-output pairs are used for training. Hence, the number of hidden layer nodes should be approximately, four. Keeping in mind that this is just a thumb rule, five nodes are used as hidden layer nodes. W_{ji}^1 denotes weight of connection between an i^{th} node in input layer to the j^{th} node in the first hidden layer and W_{oj}^2 denotes weight of connection between the j^{th} node in the hidden layer to the o^{th} node in the output layer.

5.2. Network training

Training of ANN involves adjusting its weights and biases in each iteration so as to minimise the error between the computed output and presented (desired) output. Faster rate of convergence is always desired. Levenberg-Marquardt Back propagation algorithm approaches second-order training speed without having to compute the Hessian matrix [18], [28] which can be approximated as

$$\mathbf{H} \approx \mathbf{J}^T \mathbf{J} \quad (9)$$

when the performance function has the form of a sum of squares (as is typical in training feed forward networks) and the gradient can be computed as

$$\mathbf{g} = \mathbf{J}^T \mathbf{e}. \quad (10)$$

\mathbf{J} in (9), (10) and (11) is the Jacobian matrix that contains first derivatives of the network errors with respect to the weights and biases, and \mathbf{e} is a vector of network errors. In LMBP method the Jacobian matrix can be computed through a standard back propagation technique which is much less complex than computing the Hessian matrix [28].

The LMBP algorithm uses this approximation to the Hessian matrix in the following Newton-like update:

$$\mathbf{x}_{k+1} - \mathbf{x}_k = -[\mathbf{J}^T \mathbf{J} + \mu \mathbf{I}]^{-1} \mathbf{J}^T \mathbf{e} \quad (11)$$

where \mathbf{x}_k is weight matrix or bias vector at layer k (here for ANN of Figure-8, having two layers, $k = 1$) and \mathbf{x}_{k+1} is weight matrix or bias vector at layer $k+1$ and \mathbf{e} is error vector.

In (11) when scalar μ is zero, this is just Newton's method, using the approximate Hessian matrix. When μ is large, this becomes gradient descent with a small step size. Newton's method is faster and more accurate near an error minimum, so the aim is to shift towards Newton's method as quickly as possible. Thus, μ is decreased after each successful step (reduction in performance function) and is increased only when a tentative step would increase the performance function. In this way, the performance function will always be reduced at each iteration of the algorithm.

The training goal is set to Mean Square Error (MSE) $\leq 10^{-3}$ and graph of MSE versus number of epochs

(one epoch is constitutes presentation of PT number of

input-output training pairs once) is given in Figure-9.

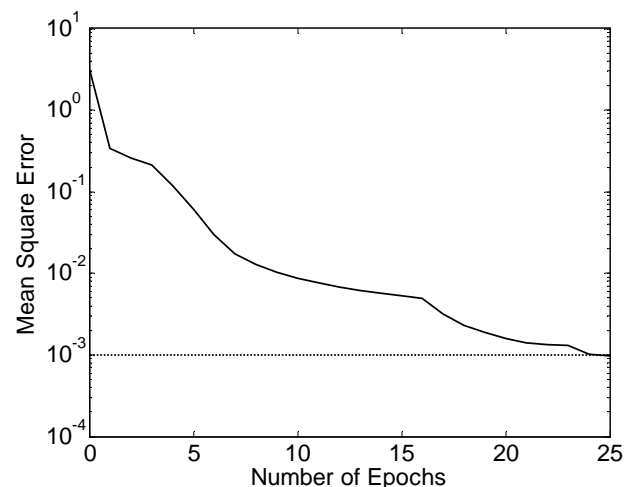


Figure-9. MSE versus No. of epochs during the training of network.

5.3 Network testing results

The results of testing the prediction using the trained ANN for some of the input parameter combinations (not used in training phase) and corresponding measured values of frequencies are given in Table-9 and plotted as function of water layer thickness in Figures 10 (a), (b) and (c). Because the predicted values of the resonant frequency are very close to the corresponding measured values of frequency, these are rounded to three digit places after the decimal point, unlike two digit places after the decimal point as given in Tables 2, 4 and 6.



Table-9. Percentage error in prediction of resonant frequency w.r.t. the measured frequency.

¹ A	² B	³ C	⁴ D	⁵ E	⁶ F	⁷ G
0	1	1.348	2	1.078	1.081	-0.3
0	4	2.136	4	1.225	1.219	0.5
0	6	3.974	0	3.974	3.943	0.78
1.524	1	1.348	1	1.264	1.272	-0.68
1.524	2	1.724	3	1.554	1.564	-0.6
1.524	4	2.136	1	2.031	2.017	0.69
1.524	5	2.6	1	2.487	2.467	0.81
1.524	5	2.6	2	2.44	2.443	-0.09
1.524	5	3.072	3	2.879	2.893	-0.48
1.524	6	3.072	4	2.858	2.857	0.03
1.524	8	3.974	2	3.83	3.879	-1.27
1.524	8	3.974	4	3.793	3.829	-0.94
1.524	9	4.554	5	4.399	4.441	-0.95
1.524	10	5.331	0	5.31	5.296	0.26
3.05	2	1.724	1	1.635	1.64	-0.27
3.05	2	1.724	2	1.607	1.612	-0.25
3.05	3	1.926	1	1.83	1.821	0.47
3.05	6	3.072	3	2.905	2.892	0.45
3.05	7	3.543	0	3.49	3.47	0.56
3.05	8	3.976	3	3.828	3.875	-1.22
3.05	8	3.976	5	3.799	3.788	0.29
3.05	9	4.554	3	4.432	4.487	-1.26
3.05	9	4.554	5	4.414	4.412	0.05
3.05	10	5.331	1	5.276	5.246	0.57

¹A = Radome thickness (mm)
²B = Antenna number
³C = Resonant frequency of antenna (GHz)
⁴D = Water layer thickness (mm)
⁵E = Measured resonant frequency (GHz)
⁶F = Resonant frequency predicted using ANN (GHz)
⁷G = Percentage error in prediction of resonant frequency w. r. t. measured frequency

From Table-9, it is observed that for 98% of test data values, the magnitude of percentage error in prediction of resonant frequency using ANN is less than 1%. The maximum error in prediction is 1.27% for the test data used.

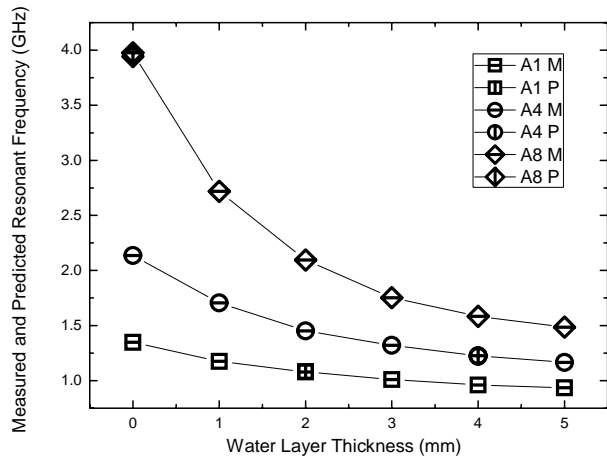


Figure-10(a). Measured and predicted values of resonant frequency for patch antennas without radome.

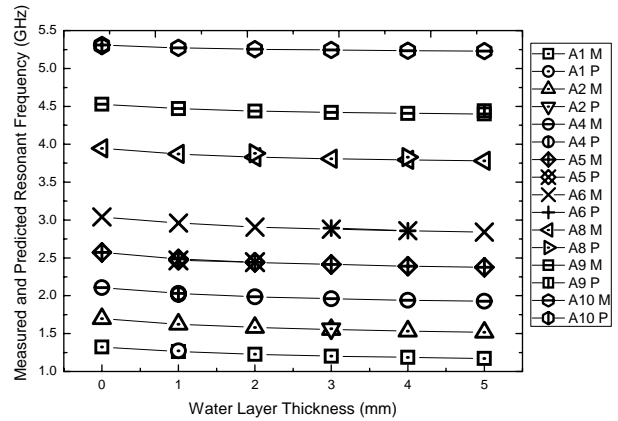


Figure-10(b). Measured and predicted values of resonant frequency for patch antennas covered with RT Duroid radome.

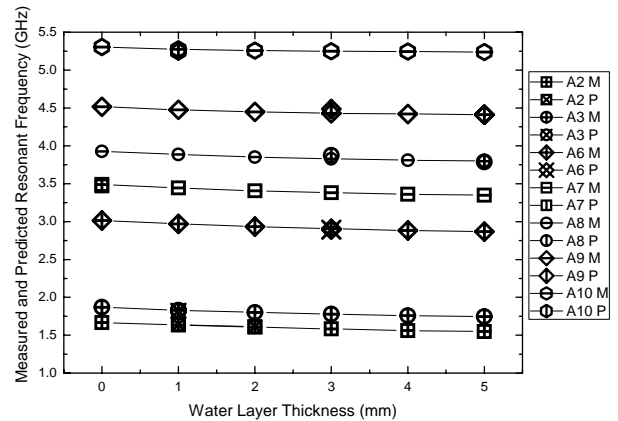


Figure-10 (c). Measured and predicted values of resonant frequency for patch antennas covered with teflon radome



6. CONCLUSIONS

The effect on the resonant frequency of rectangular patch antenna – such as one mounted flush with rooftop of a vehicle – due to accumulation of water over patch surface or its radome, in rainy condition, is studied. Empirical expressions for frequency as a function of water layer thickness for water accumulated over patch surface or over radome are presented. The resonant frequency of antenna decreases exponentially with increase in water layer thickness. The initial rate of decrease of resonant frequency in case of antennas not covered by radome is much higher compared to that of antennas covered with radome. Use of radome (which is flush with patch surface) significantly reduces the shift in resonant frequency of antenna due to accumulation of water over its radome surface. Accumulation of water also affects the impedance matching of probe-feed with patch antenna, which tends to become worse, both for antennas without radome and with radome. Multilayer Perceptron type Artificial Neural Network, trained using Levenberg-Marquardt Back propagation algorithm is presented as generalized model and better alternative to the set of empirical expressions for resonant frequencies. The results of resonant frequency of patch antenna due to accumulation of water over its patch or radome surface, predicted by trained ANN are in very good agreement with the measured ones.

REFERENCES

- [1] R. Garg, I. J. Bahl, P. Bhartia and A. Ittipiboon. 2001. *Microstrip Antennas Design Handbook*. Artech House, Boston, MA. Ch. 1.
- [2] Inder J. Bahl, Prakash Bhartia, Stanislaw S. Stuchly. 1982. Design of microstrip antennas covered with a dielectric layer. *IEEE Transactions on Antennas and Propagation*. 30(2): 314-318.
- [3] Thomas Meissner and Frank J. Wentz. 2004. The complex dielectric constant of pure and sea water from microwave satellite observations. *IEEE Transactions on Geosciences and Remote Sensing*. 42(9): 1836-1849.
- [4] G. A. Vidulich, D. F. Evans and R. L. Kay. 1967. The Dielectric Constant of Water and Heavy Water between 0 and 40 °C. *The Journal of Physical Chemistry*. 71(3): 656-662.
- [5] Martin Chaplin. Water structure and science. Online available: <http://www1.lsbu.ac.uk/water/microwave.html>.
- [6] William L. Marshall. 2008. Dielectric constant of water discovered to be simple function of density over extreme ranges from - 35 to + 600 °C and to 1200 mpa (12000 atm.), believed universal. *Nature Proceedings*: doi: 10.1038/npre. 2008.2472.1, November 4, pp. 1 - 40.
- [7] I. J. Bahl and Stanislaw S. Stuchly. 1980. Analysis of a microstrip covered with a lossy dielectric. *IEEE Transactions on Microwave Theory and Techniques*. 28(2): 104-109.
- [8] Nicólaos G. Alexópoulos and David R. Jackson. 1984. Fundamental superstrate (cover) effects on printed circuit antennas. *IEEE Transactions on Antennas and Propagation*. 32(8): 807-816.
- [9] J. Pribetich R. Ledee P. Kennis P. Pribetich M. Chive. 1988. Modelling of microstrip antenna with dielectric protective layer for lossy medium. *Electronics Letters*. 24(23): 1464-1465.
- [10] J. Svačina. 1992. Analysis of multilayer microstrip lines by a conformal mapping method. *IEEE Transactions on Microwave Theory and Techniques*. 40: 769-772.
- [11] O. M. Ramahi and Y. T. Lo. 1992. Superstrate effect on the resonant frequency of microstrip antennas. *Microwave and Optical Technology Letters*. 5: 254-57.
- [12] A. Verma and Z. Rostamy. 1993. Resonant frequency of uncovered and covered rectangular microstrip patch using modified Wolff model. *IEEE Transactions on Microwave Theory and Techniques*. 41: 109-116.
- [13] S. S. Zhong, G. Liu and G. Qasim. 1994. Closed form expressions for resonant frequency of rectangular patch antennas with multidielectric layers. *IEEE Transactions on Antennas and Propagation*. 42: 1360-1363.
- [14] Jennifer T. Bernhard and Carolyn J. Tousignant. 1999. Resonant frequencies of rectangular microstrip antennas with flush and spaced dielectric superstrates. *IEEE Transactions on Antennas and Propagation*. 47(2): 302-308.
- [15] Harold A. Wheeler. 1964. Transmission-line properties of parallel wide strips by a conformal-mapping approximation. *IEEE Transactions on Microwave Theory and Techniques*. 12: 280-289.
- [16] Harold A. Wheeler. 1965. Transmission-line properties of parallel strips separated by a dielectric sheet. *IEEE Transactions on Microwave Theory and Techniques*. 13: 172-185.
- [17] C. Christodoulou and M. Georgiopoulos. 2001. *Applications of Neural Networks in Electromagnetics*. Artech House, Boston, MA.



www.arnpjournals.com

- [18] S. Haykins. 1994. *Neural Networks: A Comprehensive Foundation*. IEEE Computer Society Press, New York, USA.
- [19] Rajeev R. Wakodkar, Bhaskar Gupta and Samik Chakraborty. Variation of resonant frequency of a rectangular microstrip patch antenna due to accumulation of water over its surface. 2010. International Conference on Applications of Electromagnetism and Student Innovation Competition Awards (AEM2C). pp. 239-243. 10.1109/AEM2C.2010.5578769
- [20] IE3D Electromagnetic simulator. 2004. Zeland Software Inc., USA. Release 10.12.
- [21] James J. R. and P. S. Hall (Eds). 1989. *Handbook of Microstrip Antennas*. IEE Electromagnetic Waves Series 28. Peter Peregrinus Ltd., London.
- [22] A. Bhattacharyya and T. Tralman. 1988. Effects of dielectric superstrate on patch antennas. *Electronics Letters*. 24: 356-358.
- [23] A. Patnaik, D. Anagnostou, R. K. Mishra C. G. Christodoulou and J. C Lyke. 2004. Applications of neural networks in wireless communications. *IEEE Antennas and Propagation Magazine*. 46(3): 130-137.
- [24] A. Patnaik and R. K. Mishra. 2000. ANN techniques in microwave engineering. *IEEE Microwave Magazine*. 1(1): 55-60.
- [25] Lucio Vegni and Alessandro Toscano. 1997. Analysis of microstrip antennas using neural networks. *IEEE Transactions on Magnetics*. 33(2): 1414-1419.
- [26] R. K. Mishra and A. Patnaik. 1998. Neural network-based CAD model for the design of square-patch antennas. *IEEE Transactions on Antennas and Propagation*. 46(12): 1890-1891.
- [27] R. K. Mishra and A. Patnaik. 2003. Designing rectangular patch antenna using the neurospectral method. *IEEE Transactions on Antennas and Propagation*. 51(8): 1914-19221.
- [28] Hagan M. T. and M. B. Menhaj. 1994. Training feed forward networks with the Marquardt algorithm. *IEEE Transactions on Neural Networks*. 5(6): 989-993.